Physics of Fluids

Kinematic stability and simulations of the variational two-fluid model for slug flow

Cite as: Phys. Fluids **34**, 043301 (2022); https://doi.org/10.1063/5.0086196
Submitted: 23 January 2022 • Accepted: 11 March 2022 • Published Online: 01 April 2022

A. Clausse, K. Chetty, J. Buchanan, et al.

Physics of Fluids ARTICLE scitation.org/journal/phf

Kinematic stability and simulations of the variational two-fluid model for slug flow

Cite as: Phys. Fluids **34**, 043301 (2022); doi: 10.1063/5.0086196
Submitted: 23 January 2022 · Accepted: 11 March 2022 ·
Published Online: 1 April 2022

A. Clausse,[1] K. Chetty,[2] J. Buchanan,[3] R. Ram,[4] and M. Lopez de Bertodano[4,a)]

AFFILIATIONS

[1]CNEA-CONICET and National University of Central Buenos Aires, Tandil, Argentina
[2]Advanced Cooling Technologies, Inc., Lancaster, Pennsylvania 17601, USA
[3]Naval Nuclear Laboratory, West Mifflin, Pennsylvania 15122, USA
[4]School of Nuclear Engineering, Purdue University, West Lafayette, Indiana 47907, USA

[a)]**Author to whom correspondence should be addressed:** bertodan@purdue.edu

ABSTRACT

The two-fluid short-wave theory (TF-SWT) mode of the one-dimensional two-fluid model (TFM) [A. Clausse and M. Lopez de Bertodano, "Natural modes of the two-fluid model of two-phase flow," Phys. Fluids **33**, 033324 (2021)] showed that the incompressible kinematic and Kelvin–Helmholtz instabilities are the source of the long-standing ill-posed question. Here, the stability of the short wave mode is analyzed to obtain an unstable incompressible well-posed TFM for vertical slug flow, where inertial coupling and drag play the key role. Then, a computational method is implemented to perform non-linear simulations of slug waves. Linear stability analyses, i.e., characteristics and dispersion, of a variational TF-SWT for vertical slug flows are presented. The current TFM is constituted with a lumped-parameter model of inertial coupling between the Taylor bubble and the liquid. A characteristic analysis shows that this conservative model is parabolic, and it provides a base upon which other models can be constructed, including short-wave damping mechanisms, like vortex dynamics. The dispersion analysis shows that depending on the interfacial drag, the problem can be kinematic unstable. A new kinematic condition in terms of the inertial coupling and the interfacial drag is derived that is consistent with previous theoretical and experimental results. The material waves, which are predicted by linear stability theory, then develop into nonlinear slug waveforms that are captured by the numerical simulations. These and the horizontal stratified flow waves of previous research illustrate the TFM capability to model interfacial structures that behave like waves. Otherwise, when the physics of the TF-SWT waves is ignored, the model is ill-posed.

I. INTRODUCTION

While two-fluid model (TFM) computational fluid dynamics has made significant advances in recent years,[1] together with the associated modeling of two-phase turbulence,[2] Vaidheeswaran and Lopez de Bertodano[3] demonstrated that the TFM stability difficulties remain unchanged in 3D vs 1D; they simply move to a smaller scale. Furthermore, early and recent attempts to resolve the ill-posed TFM condition[4] may be construed as mathematical or numerical artificial regularizations that do not address the fundamental short wave instabilities that arise from the TFM derivation starting from first principles. On the other hand, the short wave stability problem becomes self-evident with the new two-fluid short-wave theory (TF-SWT) formulation.

A new variational TFM formulation by Clausse and Bertodano,[5] based on the volumetric and drift fluxes, revealed its two natural modes. The resulting momentum equations are the drift-flux model (DFM) equation of Ishii[6] and the TF-SWT equation of Pauchon and Smereka,[7] which reduces to shallow-water theory as an asymptotic case. The TF-SWT addresses the long-standing ill-posed problem[8] because the kinematic and Kelvin–Helmholtz (KH) instabilities are the source of it and may be resolved with appropriate short-wave physics pertaining to these instabilities.[9] Therefore, the identification of the TF-SWT mode clarifies both the ill-posed problem and its physically based solutions. Since the DFM mode is well-posed hyperbolic,[9] the current analyses are focused on the TF-SWT equation stability only.

The KH stability of horizontal wavy flow was analyzed previously by the authors.[10] In that case, surface tension and viscosity played the key role in the linear and nonlinear stabilities of the local waves, respectively. In the present work, the kinematic stability of the short

wave mode is analyzed to obtain an unstable incompressible well-posed TFM for vertical slug flow, where it is shown that inertial coupling and drag play the key role. Furthermore, the versatility of the full TFM for all types of two-phase flow waves is illustrated by the analysis of acoustic waves[11] in bubbly flows, where the same mechanisms are also significant.

While the mechanistic derivation of the TFM is ubiquitous in engineering practice, the variational approach, first derived by Geurst,[12] has been presented in scientific publications only. When the inertial mechanisms are included on an *ad hoc* mechanistic basis, Wallis[13] demonstrated that there is an issue of objectivity with well-known potential flow solutions, e.g., accelerating flow around a sphere. The relevance of the variational TFM then is that the inertial coupling of the phases is clearly defined in terms the flow topology used to constitute the model, and it is inherently objective. Wallis[14] applied the variational technique to derive the inertial coupling for various flow configurations. In particular, he obtained the potential slug flow coupling using a lumped-parameter approach. Clausse and Bertodano[5] identified the importance of the inertial coupling model of Wallis[14] for slug flow TFM stability. The present work is a further exploration of this topic.

Characteristic analyses of the TFM are commonplace; in particular, Ramshaw and Trapp[15] showed that surface tension makes a TFM for separated flow well-posed, and Geurst[12] showed that inertial coupling does the same in bubbly flow. Although less common, TFM dispersion analyses have also been performed, e.g., the kinematic shallow-water theory stability analysis for horizontal stratified two-phase flow.[9] In the present analysis, the kinematic instability analysis is extended to slug flow, and it is shown that slugging begins when the kinematic wave speed exceeds the void wave propagation speed. A new two-phase formulation of the kinematic condition, involving both inertial coupling and interfacial drag, is obtained from the TF-SWT equations.

The bubbly to slug flow kinematic transition has also been investigated experimentally. For example, Saiz-Jabardo and Bouré[16] identified two waves, i.e., the void wave and the kinematic wave, "the higher speed wave (kinematic) being closely correlated with the appearance of slugs." They also proposed the instability condition $c_2 - v_g > 0$, which is equivalent with the analytic condition, $v_w - V_{gj} > 0$, obtained in the present work. Park *et al.*[17] later confirmed this result by measuring the amplification of the void waves. However, a two-phase theory for the kinematic instability is missing.

Nonlinear numerical simulations of the mechanistic 1D TF-SWT have been performed by the authors for horizontal wavy flow and vertical bubbly flow, using a second order numerical method with a flux limiter.[9] The same code has been modified and is used in the present work with the variational TFM. The verification of the numerical TFM method is generally performed with the well-known water faucet shallow-water theory problem of Ransom,[18] which involves the propagation of a kinematic discontinuity. A new TF-SWT verification problem with the inertial coupling of Wallis[14] has the advantage that it removes the two-phase KH instability, which is a limitation of the water faucet problem[9] when the mesh is refined. A secondary objective of the current work is to carry out this verification in terms of the Lax equivalence theorem.[19] According to Roache,[20] "verification is solving the equations right; validation is solving the right equations." This work is focused on verification.

This paper outline is as follows. First, the TF-SWT is presented as one mode of the full variational TFM,[5] which may be analyzed independently for the case of fixed volumetric flux. A characteristic analysis of the conservative TF-SWT equations with the lumped parameter slug flow inertial coupling of Wallis[14] then shows that the model is parabolic. Third, the dispersion analysis with interfacial drag is performed to demonstrate that, depending on the correlation, a well-posed unstable model may be obtained. Finally, a nonlinear simulation with the verified numerical model, including inertial coupling and drag and surface tension, shows the appearance of slug flow pulse waves that are bounded. Appendix A shows that the conservative TF-SWT momentum equation may be simplified further into a Burgers equation that is decoupled from the void propagation equation for the specific case of negligible density ratio. Since Burgers equation has an analytic solution, it enables the numerical verification of the TF-SWT computational model, and the stability of the numerical method is demonstrated by a mesh convergence test. Appendix B shows the derivation of the TF-SWT model for the Wallis topology of slug flow.[14]

II. MODEL EQUATIONS

We start with the TF-SWT derived by Clausse and Bertodano.[5] The model is valid for a 1D incompressible two-fluid flow with constant volumetric flux j; that is why it is also called the fixed-flux model.[9] Then, the virtual power principle, which generalizes the variational formulation to include dissipative flows in a consistent way, gives the following set of equations for the void fraction, α_2, and the drift flux, J, in a vertical channel,[1]

$$\frac{D\alpha_2}{Dt} + \frac{\partial J}{\partial x} = 0, \tag{1}$$

$$\frac{D\Gamma J}{Dt} - \frac{\partial}{\partial x}\left(\frac{1}{2}\Gamma' J^2\right) = F, \tag{2}$$

where $D/Dt = \partial/\partial t + j\partial/\partial x$, $\alpha_1 = 1 - \alpha_2$, and the subscript α refers to the derivative with respect to α_2. The two-fluid inertia, Γ, is written in dimensionless form as

$$\Gamma = \frac{r}{\alpha_2} + \frac{1}{\alpha_1} + \frac{m(\alpha_2)}{\alpha_1^2\alpha_2^2}, \tag{3}$$

where $r = \rho_2/\rho_1$ and $m(\alpha_2)$ is an algebraic function representing the inertial coupling between phases. The lumped-parameter model of inertial coupling for slug flow is (see Appendix B)

$$m(\alpha_2) = \left(\frac{\alpha_s - \alpha_2}{1 - \alpha_s}\right)(1 - \alpha_2)\alpha_2, \tag{4}$$

where α_s is the void fraction in the section containing the Taylor-bubble (see Fig. 12).

The interfacial force term in the momentum equation is given by

$$F = (1 - r)g - \sigma^* \frac{\partial^3 \alpha_2}{\partial x^3} - \frac{1}{2}\frac{C_D}{D} u_r |u_r|. \tag{5}$$

The first term is the buoyancy force. The second term is the surface tension force, which here is modeled following the expression derived in Ref. 9, assuming a valid direct extension of the formula for stratified flow. The resulting coefficient is given by $\sigma^* = \sigma D/\rho_1$, where σ is the surface tension and D is the pipe diameter. The last term is the interfacial drag, where the relative velocity, $u_r = u_2 - u_1$, should be later

expressed in terms of the state variables, namely, $u_r = J/(\alpha_2\alpha_1)$. C_D is a dimensionless interfacial-drag coefficient, which is generally measured in steady-state conditions by correlating its effects with the state-variables. This coefficient will be discussed in Sec. III C.

Equations (1)–(3) reduce to the Saint Venant equations for horizontal flow when $m(\alpha_2) = 0$, $r = 0$, $j = 0$, and $F = gD\frac{\partial \alpha_1}{\partial x}$ is the hydrostatic term. Therefore, the mathematics of the TF-SWT equations is similar to that of shallow-water theory, so the existing mathematical stability analysis of Whitham's[21] is used in the present work.

III. LINEAR STABILITY

A. Characteristic analysis

In engineering practice, the ill-posed condition of the Euler 1D TFM has been dealt with either significant numerical viscosity or artificial closure models. In particular, the first-order upwind (FOU) method with coarse mesh sizes is generally used. The presence of excessive numerical diffusion from the FOU scheme leads to damping of the local material or void waves, which are important for dynamic predictions of two-phase instabilities. Another common technique used is the addition of artificial interfacial momentum transfer terms, which affect the mathematical nature of the TFM governing equations, rendering them well-posed. However, once the role of the TF-SWT has been identified from energetic variational means, the derivation of physical constitutive models pertaining to specific flow regimes may be used instead. Moreover, the variational formulation satisfies objectivity, i.e., frame invariance, which complicates the mechanistic force-based derivation of the TFM and is seldom addressed.

The characteristics are found by linearizing the TF-SWT equations, i.e., Eqs. (1) and (2), with zero on the right-hand side, around the general steady state $\alpha = \alpha_o$ and $J = J_o$ for the state variables $\underline{\phi} = [\alpha_2, J]^T$, that is

$$\boldsymbol{A}\frac{\partial}{\partial t}\underline{\phi} + \boldsymbol{B}\frac{\partial}{\partial x}\underline{\phi} = 0. \tag{6}$$

Solving the characteristic equation, $Det[\boldsymbol{B} - c\boldsymbol{A}] = 0$ results in the eigenvalues c

$$c = j_o + \frac{\Gamma_o' \pm \sqrt{\Delta}}{\Gamma_o} J_o, \tag{7}$$

where the subscript "o" means that the quantity is evaluated at the steady state, and the prime indicates the derivative with respect to α_2.

It can be shown that the discriminant, Δ, for Eqs. (3) and (4) is[1]

$$\Delta = \Gamma_o'^2 - \frac{1}{2}\Gamma_o\Gamma_o'' = 0. \tag{8}$$

This leads to the following simplification of the eigenvalues:

$$c = j_o - \frac{\Gamma_o'}{\Gamma_o} J_o = j_o + V_{gj}, \tag{9}$$

where V_{gj} is the drift flux velocity of Zuber and Findlay.[22] Thus, the speed of the void waves is $c = u_{2o}$, i.e., the unperturbed gas phase velocity. Since $\Delta = 0$ for the lumped-paremeter slug flow, the model is parabolic, and the non-dimensional eigenvalues $c^* = (c - j_o)/V_{gj}$ are simply $c^*_{1,2} = 1$. Therefore, the inertial coupling of Wallis[14] eliminates the elliptic character of the TFM equations, providing a physical base to address the TFM ill-posed condition without artificial regularization.

B. Dispersion analysis

The role of the non-conservative drag force leads to an instability, closely related to the kinematic instability of Whitham for single phase shallow-water theory.[21] The surface tension is also considered in the analysis because the instability is otherwise ill-posed.

The dispersion relation is obtained from the perturbation of $\underline{\phi} = \underline{\phi}_o + \delta\underline{\phi}_o\, e^{i(kx-\omega t)}$. The linearized equations can now be written as

$$\boldsymbol{A}\frac{\partial}{\partial t}\delta\underline{\phi} + \boldsymbol{B}\frac{\partial}{\partial x}\delta\underline{\phi} + \boldsymbol{C}\frac{\partial^3}{\partial x^3}\delta\underline{\phi} + \boldsymbol{F_\phi}\delta\underline{\phi} = 0. \tag{10}$$

The coefficient matrices for Eq. (10) are given in Appendix C. Using the notation in Ref. 5, the following dispersion relation for the material waves is then obtained:

$$\omega = j_o k - \frac{\Gamma'}{\Gamma} J k - i\frac{F_U}{2} \pm \sqrt{\left(i\frac{F_U}{2}\right)^2 + \frac{iF_{\alpha_2}k + \sigma^* k^4}{\Gamma}}, \tag{11}$$

where $U = \Gamma J$, $F_U = \frac{\partial F}{\partial U}$, and $F_{\alpha_2} = \frac{\partial F}{\partial \alpha_2}$. In Sec. III A, the radical was zero but now it depends on Γ, F, and σ, and the problem is unstable. The dispersion relation may be written in more conventional terms to show the association of the current instability with the kinematic shallow-water instability of Whitham.[21] Starting with the definition of the kinematic velocity in two-phase flow,

$$v_w = \left.\frac{\partial J}{\partial \alpha_2}\right|_F = -\frac{F_{\alpha_2}}{F_J} = -\frac{1}{2}\frac{C_D^{*\prime}}{C_D^*} J, \tag{12}$$

where $C_D^* = C_D/D_{pipe}\alpha_2{}^2(1-\alpha_2)^2$, it follows that

$$v_w - V_{gj} = -\frac{F_{\alpha_2}}{\Gamma F_U} = \left(-\frac{1}{2}\frac{C_D^{*\prime}}{C_D^*} + \frac{\Gamma'}{\Gamma}\right) J, \tag{13}$$

so the dispersion relation has the same form as Whitham's

$$\omega = (j_o + V_{gj})k - \left[i\frac{F_U}{2} \pm \sqrt{\left(i\frac{F_U}{2}\right)^2 - i(v_w - V_{gj})F_U\, k + \frac{\sigma^*}{\Gamma}k^4}\right]. \tag{14}$$

The first term on the RHS corresponds to the characteristic wave speed of Sec. III A, and the terms in square brackets emerge from the addition of interfacial drag and surface tension. In this particular case of vertical slug flow, the significant hydrostatic term of horizontal flow is not present, so the dispersion relation is not exactly the same as Whitman's shallow-water theory result.[21] The instability condition, $v_w - V_{gj} > 0$, acquires a new two-fluid formulation given by Eq. (13), but the kinematic instability is essentially the same in the sense that it corresponds with the two waves observed experimentally.[16,17] Furthermore, the effect of the size and shape of the bubbles on the transition, also observed experimentally,[23] becomes clear from the new formulation since the inertial coupling and the drag strongly depend on them.

For the current model, the inertial problem is at the verge of instability, i.e., it is parabolic, and then the kinematic term, $(v_w - V_{gj})$,

makes the problem unstable. Furthermore, the wave growth rate becomes infinity at zero wavelength without surface tension, unlike single phase shallow-water theory, i.e., for $k \to \infty$ then $\omega_i \to \infty$. However, the linear stabilization of the TFM, first published by Ramshaw and Trapp,[15] may be obtained adding surface tension, i.e., the last term in Eq. (14) suppresses the wave growth for wavenumbers higher than those of the capillary waves. The model then becomes well-posed dispersive,[21] i.e., the wave speed depends on the wave number. Thus, the traditional classification of partial differential equations is insufficient to describe the complexities of this mode of the TFM, but the more recent classification of Whitham[21] may be used. Furthermore, since the DFM mode of the TFM is always hyperbolic,[9] the local stability difficulties of the TFM are shown to belong to the TF-SWT mode only. Finally, since the linear stability theory of the DFM is well-understood,[24] the current analysis complements the fluid dynamic understanding of the stability of the full TFM.

C. Slug flow stability

The 1D variational TF-SWT requires a constitutive model for the non-conservative (dissipative) interfacial drag force in addition to the conservative inertial forces. The interfacial drag force is discussed in this section since it determines whether the 1D variational TF-SWT is unstable, giving rise to the growth of slug flow waves. A drag coefficient C_D was obtained from the experimental data of Cheng *et al.*[23] using a force balance between interfacial drag and buoyancy. This C_D accounts for the dispersed, clustered bubbly and slug flow regimes. For the drag coefficient, C_D, given below in Eq. (15), the relative velocity $u_r = u_2 - u_1$ was calculated using the reported values of void fraction α_2 and the gas and liquid volumetric fluxes, i.e., $j_2 = \alpha_2 u_2$ and $j_1 = (1-\alpha_2)u_1$, respectively,

$$C_D^{\exp} = 2\, e^{-29.41\alpha^4+61.26\alpha^3-48.61\alpha^2+9.33\alpha+1.32}. \tag{15}$$

For comparison, the drag coefficient of Ishii and Chawla[25] for slug flow is given by

$$C_D^{slug} = 9.8\,(1-\alpha_2)^3. \tag{16}$$

The experimentally derived C_D differs from the drag coefficient C_D^{slug} as shown in Fig. 1. It can be seen that $C_D^{\exp}$ is close to C_D^{slug} for the average void fraction range of $\alpha_2 \geq 0.5$.

The drag coefficient of Ishii and Chawla[25] for churn flow is also of interest to the stability of the model:

$$C_D^{churn} = \frac{8}{3}(1-\alpha_2)^2 \tag{17}$$

and, following the trend, one may propose a general drag coefficient of the form:

$$C_D = C_{D\infty}\,(1-\alpha_2)^n. \tag{18}$$

The dispersion relation obtained with the experimental drag coefficient is shown in Fig. 2. The model with surface tension is well-posed,[15] i.e., for $k \to \infty$, $\omega_i \to 0$.

To explain why the model simulations result in pulse waves, it is necessary to look into the form of the drag coefficient. In single-phase flow, the growth rate of the kinematic shallow-water theory instability is dependent on the slope of the drag force, and the same applies for the 1D variational TF-SWT. When Ishii's slug-flow drag correlation, Eq. (16), is used, the relative kinematic wave speed, Eq. (13), is positive for all void fractions, as shown in Fig. 3, so the TFM is unstable. However, when the experimental drag is used, the figure shows that the problem becomes stable for low and high void fraction so it is bi-stable, leading to the topology of slug flow. Furthermore, for the churn flow correlation of Ishii and Chawla, Eq. (17), the TFM becomes exactly stable due to the simple formulations of the constitutive models, i.e., Eqs. (4) and (17). This clearly does not happen in reality, and therefore, a more advanced model would be necessary. Furthermore, it is clear from Fig. 3 that the model becomes stable for $n < 2$ in Eq. (18), and that the stability may be controlled changing n. So, the

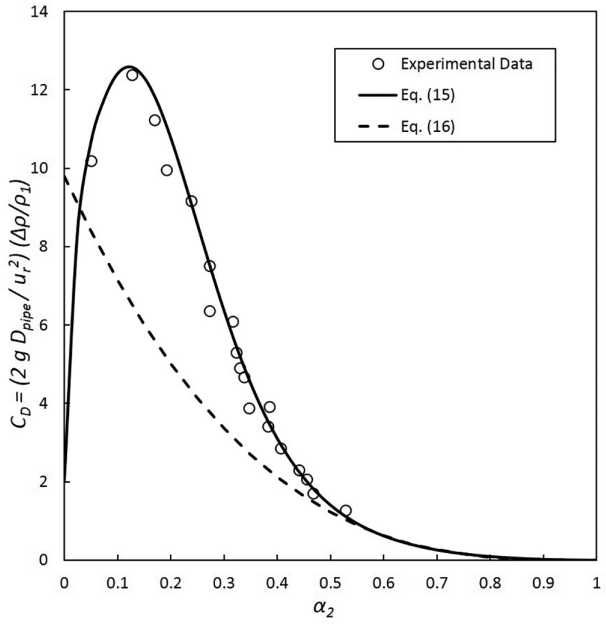

FIG. 1. Experimental interfacial drag coefficient based on force balance between drag and gravity.

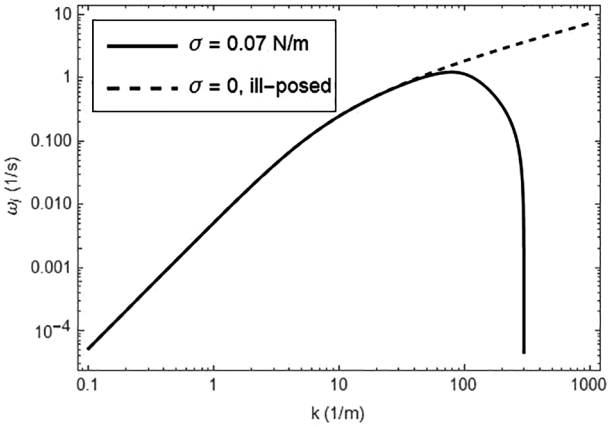

FIG. 2. Dispersion relation for $\alpha_2 = 0.5$.

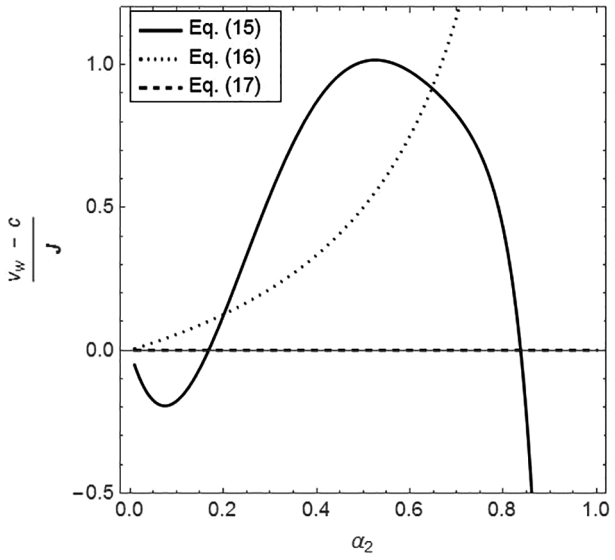

FIG. 3. Kinematic relation, Eq. (13).

formulation of the drag force allows the regularization of the TFM if short waves are undesirable or if the flow regime is stable. However, removing the short waves for unstable flow begs the question of the necessity of the TFM vs the DFM.

D. Film flow stability

Assuming constant α_s, the lumped-parameter geometry of slug-flow is not valid for void fractions higher than α_s. Instead, the inertia and the drag can be modified such that $v_w - V_{gj} = 0$ beyond $\alpha_s = 0.92$, so the film model becomes stable. The modified inertia is $m(\alpha_2) = 0$, so there is no coupling, and the drag coefficient is set to Wallis annular flow correlation.[26] The modified inertia is then

$$\Gamma = \frac{r}{\alpha_2} + \frac{1}{\alpha_1}, \quad \alpha_2 > \alpha_s. \tag{19}$$

We employ Eqs. (11.9) and (11.24) of Wallis[13] for the drag due to the shear stress on the wavy annular film,

$$-\frac{dp}{dx} = C_{fsg}\frac{2}{D}\rho_g j_g^2, \quad C_{fsg} = 0.005[1 + 90(1 - \alpha_2)]. \tag{20}$$

It can then be shown that the film becomes neutrally stable, i.e., the kinematic condition is precisely zero, with the approximation $C_{fsg} \cong 0.005[1 + 90(1 - \alpha_s)]$ and the inertial coupling given by Eq. (19) with $r \ll 1$. However, in the simulations shown in Sec. IV, $\alpha_2 < \alpha_s$ practically all the time, so the film flow model is addressed only for completeness.

Finally, a Dirac function in the inertial coupling was inserted to cap the void fraction in the Taylor bubble region, so $\alpha \leq 1$, given the restriction for closed channels, i.e.,

$$m_s(\alpha) = -\frac{\delta_s}{(1 - \alpha)^2}, \quad \delta_s = 10^{-4}. \tag{21}$$

IV. NONLINEAR STABILITY

A. Slug flow simulations

The equations of the 1D variational TF-SWT were solved numerically using a 1D FORTRAN code.[9] The equations are discretized using the second order finite difference method on a staggered grid arrangement using the flux limiter function based on the general piecewise limiter scheme of Waterson and Deconick.[27] The SMART flux limiter scheme was chosen due to its capability to resolve shock like structures. For time advancement, the third order Runge–Kutta scheme of Gottileb and Shu[28] was chosen. The verification of the TF-SWT computational model, in the sense of the Lax equivalence theorem, is given in Appendix A. A new Two-Fluid Burgers problem was developed to perform the verification.

The conditions of the experiment of Cheng *et al.*[23] were used for this simulation. The dimensions of the test section are $L = 4.1$ m and $D_{pipe} = 0.0289$ m. The void measurements were obtained with six impedance probes along the test section. The other measurements are two flow meters for the water and the air, and several pressure taps.

A simulation was performed with the experimental drag model of Eq. (15) and $\alpha_s = 0.92$, using the numerical code outlined above. The inlet boundary conditions are $j_{in} = 1.12\frac{m}{s}$, $\alpha_{in} = 0.523$, and $U_{in} = \Gamma J_{in} = 3.0$ m/s, i.e., $F = 0$ in Eq. (5), with a sinusoidal perturbation added to "seed" the wave growth. The node density $N = 1000$ nodes/m was shown to converge in Appendix B. The computational domain was approximately four times longer, $x \in [0, 15\,\text{m}]$ to obtain the fully developed Taylor bubbles shown in Figs. 5 and 6.

B. Discussion

The most dangerous wave number obtained with the stability theory ranges between $k = 10$ and $100\,\text{m}^{-1}$, as shown in Fig. 4. This is in agreement with the initial stage of the void fraction profile development close to the channel inlet in Fig. 5. However, as these waves develop, non-linear effects are triggered, leading toward a sustained train of soliton-like waves with longer wave lengths ($k \sim 6\,\text{m}^{-1}$).

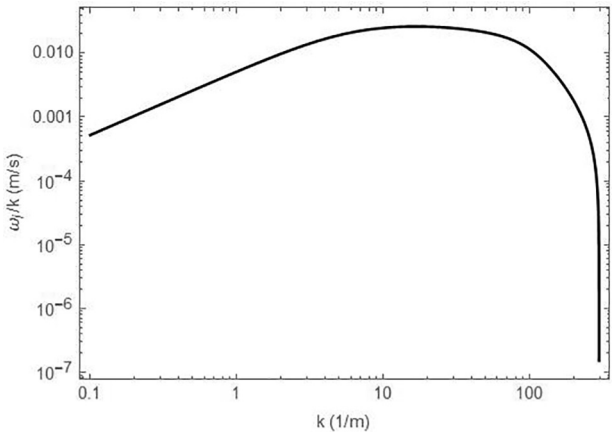

FIG. 4. Linear theory; wave growth speed.

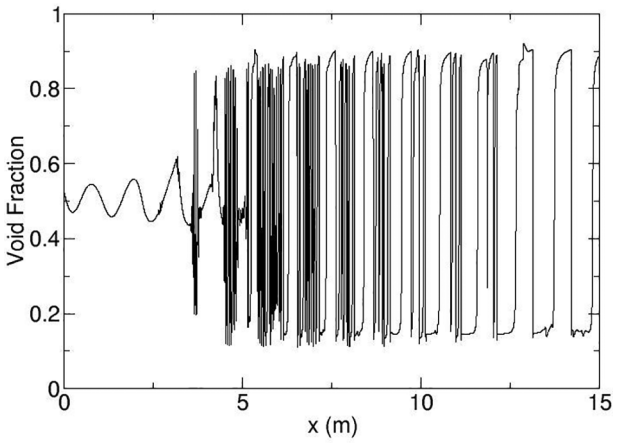

FIG. 5. Spatial distribution of void fraction pulses (α_2 vs x) from 1D TF-SWT slug flow simulations.

This is in agreement with the experimental observations[16,17] and Ref. 23. The series of pulses obtained in the numerical simulation corresponds to the linearly bi-stable conditions at low and high void fractions, i.e., 0.2 and 0.9, of the dispersion stability analysis shown in Fig. 3. The instability in the intermediate range switches the void fraction between the two stable values. The shape of the void pulses is similar to the void fraction wave obtained for the void propagation verification shown in Fig. 9. However, a computational domain of 15 m was necessary to obtain the fully developed slugs, as shown in Fig. 5.

Comparing the time series of the simulation at the exit, Fig. 6, with the time series of the experiment at the probe located at $x = 3.55$ m, Fig. 7, the height of the pulses is in agreement for $\alpha_s = 0.92$. The wavelength is also similar because of the inlet condition, which, despite the chaos in between, prevails toward the exit. However, the shape of the top of the waves differs from the experiment since the physics of the dome of the Taylor bubble is missing, as shown in Appendix B.

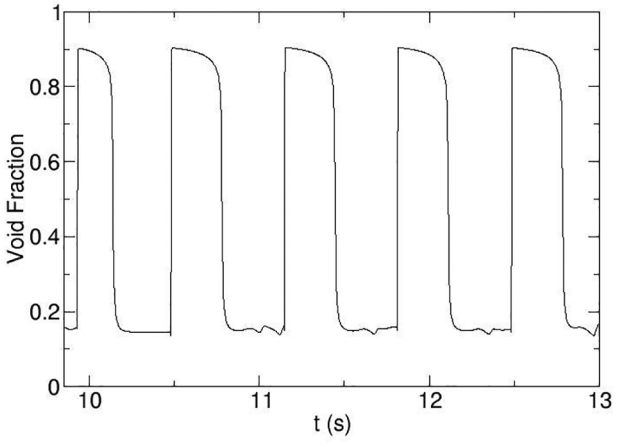

FIG. 6. Time series plot of void fraction pulses (α_2 vs t) from 1D TF-SWT slug flow simulations.

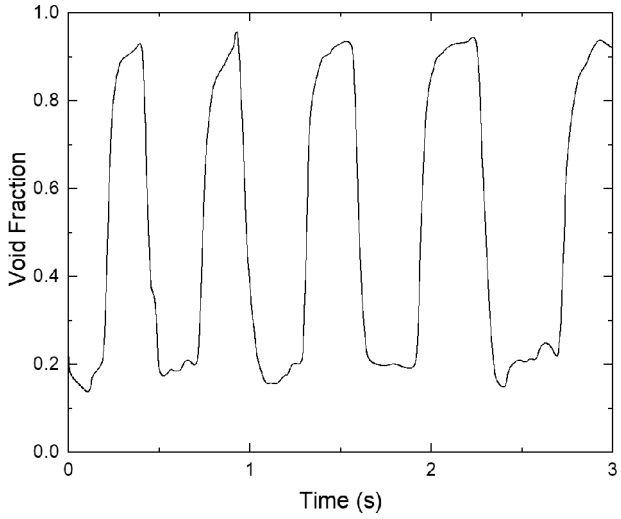

FIG. 7. Time series plot of void fraction pulses (α_2 vs t) from Cheng *et al.*[23] for slug flow.

It is clear from this discussion that the inertial-coupling model of Wallis[14] for slug flow, the only one available in the literature, is not sufficient to describe the full dynamics observed in the experiment, e.g., the long range "drafting" from the entrained vortex behind the Taylor bubble is missing. However, it is sufficient to reveal the nature of the pulses in terms of the stability theory of the novel TF-SWT approach. In particular, it allows a new definition of the kinematic condition for slug flow and the nonlinear development of the pulse waves.

V. CONCLUSIONS

This work illustrates a method to develop an unstable but physically well-posed incompressible TFM for slug flow, based on linear and nonlinear stability analyses of the TF-SWT mode. The common practice to apply artificial regularizations to force the TFM to become hyperbolic to preclude local instabilities is both unphysical and unnecessary. For instance, the current TFM is parabolic-dispersive.

The current instability is kinematic, like the well-known shallow-water theory case of single-phase flow.[21] This two-phase formulation incorporates short wave physics, i.e., inertial coupling and interfacial drag, to constitute an unstable well-posed model of the local material waves. The dispersion analysis results in a new kinematic condition that extends the kinematic stability theory of Whitham[21] to slug flow and is consistent with experiments.

The waves, which are predicted by the linear stability theory, develop into nonlinear pulse waveforms. These waveforms, corresponding to the topology of slug flow, are originally determined by the bi-stable kinematic relation between inertial coupling and the drag correlation, and the pulse form is driven by nonlinear dynamics obtained by the simulation. The dispersion analysis also shows that the drag correlation determines the overall stability of the model, so the local waves may be removed by changing it. Thus, removing the slug flow instability is a way to regularize the TFM for system analysis.

These results are only conceptual, since some relevant physics, discussed in Sec. IV B, is missing. However, the TFM simulation

obtains the topology of slug flow[1] because the interfacial waves remain embedded in the new TF-SWT formulation, even when the interfaces have been removed by the TFM averaging. So, the simulations of vertical slug flow waves and of the horizontal stratified flow waves of previous research[10] illustrate that the TFM still maintains the capability to model those interfacial structures that behave like waves. Otherwise, when this capability is ignored, the model is ill-posed.

The present model is highly ideal, and therefore, there is plenty of room for improvement. The reason for the simplicity chosen in this version is that, at the current development stage of the variational model, it is important to identify and quantify the instability mechanisms involved in slug flow. These instabilities are produced by the interplay between the interfacial drag and the inertial coupling. The latter is a non-dissipative mechanism, which can only be correctly derived from first principles by means of the variational principles of fluid mechanics. The basic lumped parameter model used in the present version is characterized by a single parameter, namely, α_s, which, for the sake of simplicity, was kept constant for all regimes. Future studies will address more sophisticated models, which may include the variation of α_s with the local void fraction and additional inertial-coupling terms due to recirculation within the representative volume element.

ACKNOWLEDGMENTS

This research was funded by Fluor Marine Propulsion, LLC, West Mifflin, Pennsylvania, PO 133569.

AUTHOR DECLARATIONS

Conflict of Interest

The authors have no conflicts to disclose.

DATA AVAILABILITY

The data that support the findings of this study are available within the article.

APPENDIX A: TWO-FLUID BURGERS EQUATION

The 1D variational TF-SWT equations without the interfacial drag and gravity for the slug flow model of Wallis[14] are re-written in terms of α_2 and $U = \Gamma J$ as

$$\frac{\partial \alpha_2}{\partial t} + \frac{\partial}{\partial x}\left(\frac{U}{\Gamma}\right) = 0, \tag{A1}$$

$$\frac{\partial U}{\partial t} - \frac{\partial}{\partial x}\left(\frac{\Gamma' U^2}{2\,\Gamma^2}\right) = 0. \tag{A2}$$

Since $r_p = \rho_2/\rho_1 \ll 1$ for an air–water two-phase mixture, the non-dimensional two-phase inertia Γ, Eq. (4), simplifies as

$$\Gamma = \left(\frac{\alpha_s}{1-\alpha_s}\right)\frac{1}{\alpha_2}, \tag{A3}$$

$$\Gamma' = -\left(\frac{\alpha_s}{1-\alpha_s}\right)\frac{1}{{\alpha_2}^2}. \tag{A4}$$

Using Eqs. (A3) and (A4), the 1D variational TF-SWT equations can be simplified as

$$\frac{\partial \alpha_2}{\partial t} + \frac{\partial \alpha_2 U}{\partial x^+} = 0, \tag{A5}$$

$$\frac{\partial U}{\partial t} + U\,\frac{\partial U}{\partial x^+} = 0, \tag{A6}$$

where $x^+ = \frac{1-\alpha_s}{\alpha_s}x$. Thus, it can be seen that the slug flow model of Wallis[14] for negligible r_p simplifies the momentum equation of the 1D variational TF-SWT equations into a two fluid Burgers equation. Furthermore, Eq. (A6) is decoupled from the void propagation equation, Eq. (A5). The significance of the Two Fluid Burgers equation lies in the fact that it has a well-known analytical solution obtained by the method of characteristics, and this enables an analytical solution for the void propagation equation as well. Therefore, these equations are used here to verify the TFM.

For the numerical simulations of the two fluid Burgers equation, a piecewise linear initial condition is chosen for U:

$$\begin{gathered} U(x^+(0),0) = U_0 = a + b\,x^+, \\ a = 2.03, \\ b = \begin{cases} -0.2, & for\ x^+ \le 0.1, \\ 0.2, & for\ 0.1 \le x^+ \le 0.2, \\ 0, & for\ x^+ \ge 0.2. \end{cases} \end{gathered} \tag{A7}$$

The analytical solution for U^* from the method characteristics is

$$U(x^+,t) = \frac{a + b\,x^+}{1 + b\,t}. \tag{A8}$$

The non-dimensional inertia Γ with the $r_p \ll 1$ simplification was implemented in the code to solve for α_2 and U. The simulations were run for 25 s. The comparisons of the simulation results with the analytical solution for different mesh sizes are shown in Fig. 8, using a piecewise initial condition for U. It can be seen that the numerical solution converges to the analytical solution as the mesh size decreases, and the initial piecewise solution for U develops a shock at the rear with an expansion wave at the front.

The next step of verification involves the void propagation equation, i.e., the continuity equation Eq. (A5) along with the Two Fluid Burgers equation, i.e., the momentum equation, Eq. (A6). As before, a piecewise initial condition is used for α_2:

$$\begin{gathered} \alpha_2(x^+(0),0) = \alpha_{20} = p + q\,x^+, \\ p = 0.5, \\ q = \begin{cases} 0.05, & for\ x^+ \le 0.1, \\ -0.05, & for\ 0.1 \le x^+ \le 0.2, \\ 0, & for\ x^+ \ge 0.2. \end{cases} \end{gathered} \tag{A9}$$

The initial condition for U is the same used in the two fluid Burgers problem. The solution for the void propagation equation follows

$$\alpha_2(x^+,t) = \frac{p + q\,x^+ + (b\,t - a\,q)t}{(1 + b\,t)^2}. \tag{A10}$$

The comparisons of the simulation results with the analytical solution for different mesh sizes for $\alpha_2(x^+,t)$ are shown in Fig. 9. It can be seen that the numerical solution converges to the analytical solution as the mesh size decreases, and the solution is unique as the initial piecewise condition for α_2 develops into a quasi-square

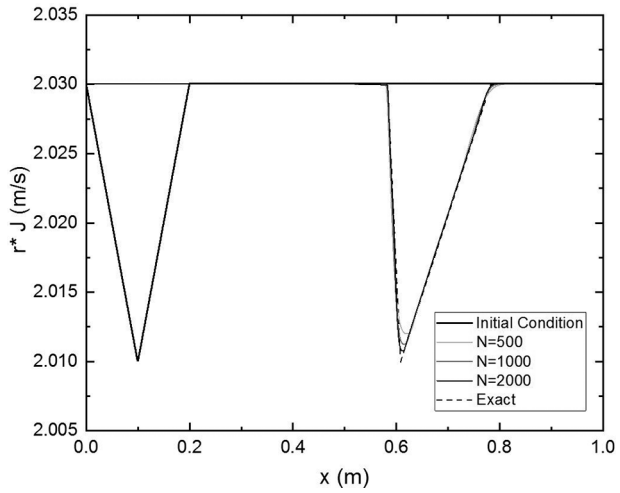

FIG. 8. Comparison of numerical solution of 1D variational TF-SWT Burgers equation with analytical solution for different grid sizes using a piecewise initial condition.

wave with three distinct material shocks. At this point, it is appropriate to compare this result with the water faucet problem, which is the standard verification of the TFM for material shocks. Unlike the current problem, the water faucet is for single phase Shallow-Water Theory, so when used for TFM verification, the mesh cannot be refined beyond a certain point because a KH instability develops at the discontinuity and the overshoot grows unbounded.[9] Nevertheless, Figs. 10 and 11 show that before that point, the code converges for the current problem at the same rate as previous simulations of the water faucet problem[9] using the same code, i.e., for problems with shocks, the rate of convergence is $\sim O(0.7)$. For smooth solutions, it has been already shown that the code has second-order convergence.[9]

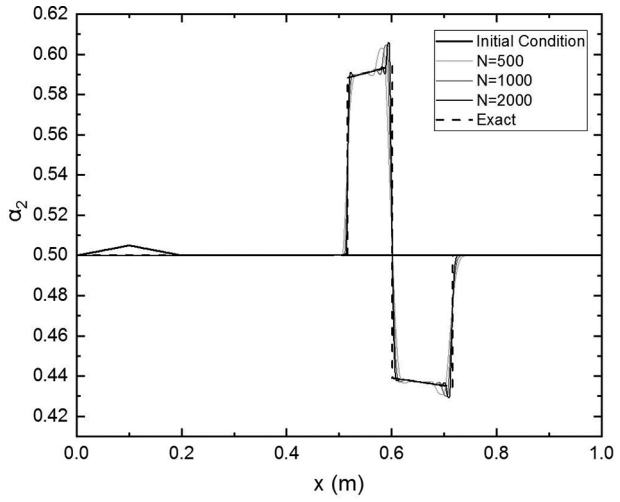

FIG. 9. Comparison of numerical solution of 1D variational TF-SWT's void propagation equation with analytical solution for different grid sizes using a piecewise initial condition.

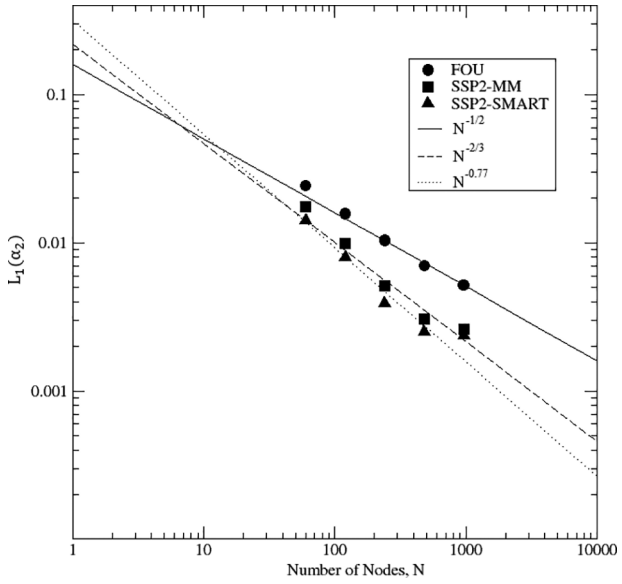

FIG. 10. Convergence rate of water faucet problem[9] with different flux-limiter schemes.

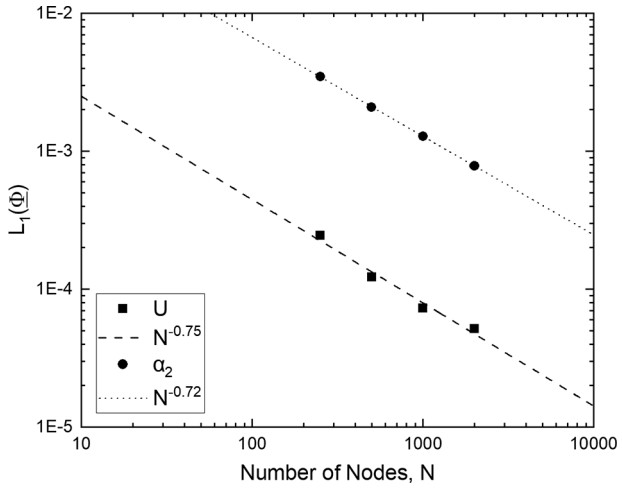

FIG. 11. Convergence rate of the two fluid Burgers problem with the SMART flux-limiter scheme.

APPENDIX B: VARIATIONAL DERIVATION OF THE WALLIS INERTIAL COUPLING COEFFICIENT

The derivation of the inertial coupling coefficient for the slug flow model of Wallis[14] is discussed here. Consider a unit cell configuration of a cylindrical bubble, representing a Taylor bubble, moving in the axial direction along with the liquid in a vertical pipe as shown in Fig. 12. The bubble moves with velocity u_2, and it occupies a fraction α_s of the cross section of the pipe. The liquid in the unit cell has two different uniform velocities: u_f in the film around the Taylor bubble and u_s in the liquid slug behind the Taylor bubble.

From Fig. 12, the volume averaged gas void fraction α_2 is

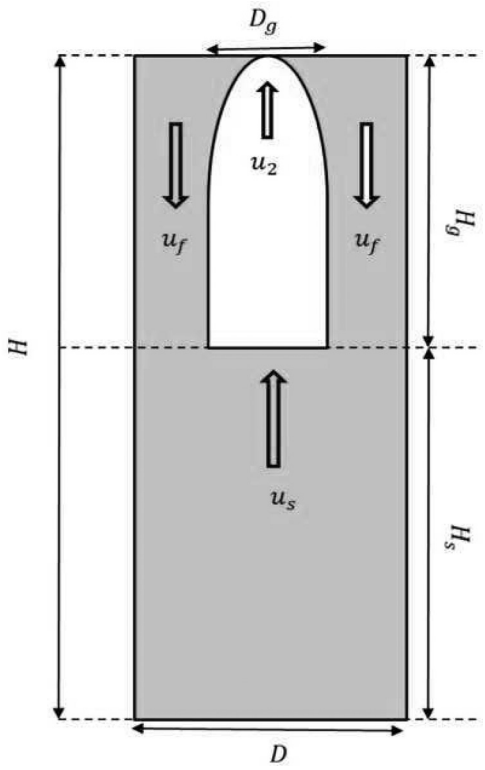

FIG. 12. Wallis' lumped parameter model for slug flows.

$$\alpha_2 = \frac{H_g D_g^2}{H D^2}. \tag{B1}$$

The fraction of the cross-sectional area of the pipe occupied by the cylindrical bubble is given by

$$\alpha_s = \frac{D_g^2}{D^2}. \tag{B2}$$

Using the fixed volumetric flux approximation (i.e., constant j), since the variational formulation ensures Galilean invariance, one can chose any inertial coordinate frame to derive the final form of inertial coupling; the relative velocity is the same in all inertial systems. Therefore, to simplify the derivation, let us chose a coordinate frame moving with velocity j, so that with respect to this frame, $j = \alpha_2 u_2 + \alpha_1 u_1 = 0$, and we have

$$\begin{aligned} u_1 &= \frac{-\alpha_2 u_2}{1-\alpha_2}, \\ u_s &= 0, \\ u_f &= \left(\frac{\alpha_s}{1-\alpha_s}\right) u_2. \end{aligned} \tag{B3}$$

Now we can define the volume averaged kinetic energy density K of the two-phase mixture in the unit cell as

$$K = \frac{1}{2}\rho_2 \alpha_2 {u_2}^2 + \frac{1}{2}\rho_1 (1-\alpha_s)\left(\frac{H_g}{H}\right){u_f}^2. \tag{B4}$$

By using the definition of drift flux $J = \alpha_1 \alpha_2 u_r$, we can write u_1, u_2, and u_f as

$$\begin{aligned} u_1 &= \frac{-J}{1-\alpha_2}, \\ u_2 &= \frac{J}{\alpha_2}, \\ u_f &= \left(\frac{-\alpha_s}{1-\alpha_s}\right)\frac{J}{\alpha_2}. \end{aligned} \tag{B5}$$

Using $H_g/H = \alpha_2/\alpha_s$, the kinetic energy density K can be rewritten as

$$K = \frac{1}{2}\frac{J^2}{\alpha_2}\left[\rho_2 + \rho_1\left(\frac{\alpha_s}{1-\alpha_s}\right)\right]. \tag{B6}$$

Following Pauchon and Smereka,[7] representing the net two-phase inertia as Γ, the kinetic energy density K can be written as

$$K = \frac{1}{2}\Gamma J^2, \tag{B7}$$

where the definition of the two-phase inertia Γ follows

$$\Gamma = \frac{\rho_2 + \rho_1\left(\frac{\alpha_s}{1-\alpha_s}\right)}{\alpha_2}. \tag{B8}$$

The definition of the inertial coupling coefficient $m(\alpha_2)$ can be obtained from the definition of Γ using the following relation:

$$\Gamma = \frac{\rho_1}{\alpha_1} + \frac{\rho_2}{\alpha_2} + \frac{\rho_1\, m(\alpha_2)}{{\alpha_1}^2 {\alpha_2}^2}. \tag{B9}$$

From Eqs. (B8) and (B9), the inertial coupling coefficient $m(\alpha_2)$ for the slug flow model of Wallis[14] is

$$m(\alpha_2) = (1-\alpha_2)\alpha_2\left(\frac{\alpha_s - \alpha_2}{1-\alpha_s}\right). \tag{B10}$$

A desirable feature of $m(\alpha_2)$ in Eq. (B10) is that it leads to zero added mass for the limiting case of $\alpha_1 = 1 - \alpha_2 = 0$ and $\alpha_2 = 0$. An undesirable feature is that it becomes negative for $\alpha_2 > \alpha_s$. Figure 13 shows the plot of $m(\alpha_2)$ for $\alpha_s = 0.92$.

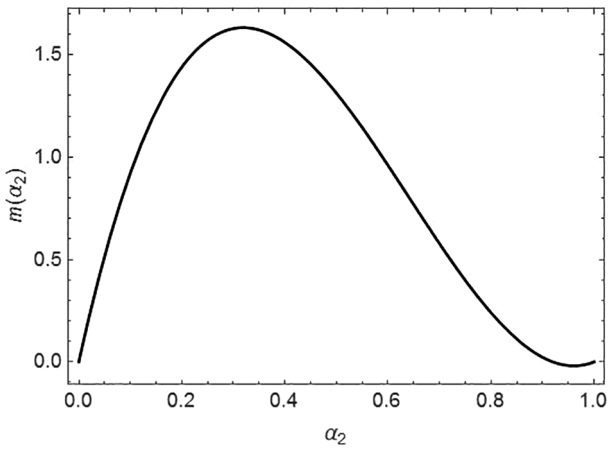

FIG. 13. Inertial coupling coefficient for the slug flow model of Wallis.[14]

APPENDIX C: COEFFICIENT MATRICES FOR LINEAR STABILITY ANALYSYS

The matrices for Eq. (10) are

$$\underline{\phi} = \begin{bmatrix} \alpha_2 \\ U \end{bmatrix}, \tag{C1}$$

$$\boldsymbol{A} = \boldsymbol{I}, \quad \boldsymbol{B} = \begin{bmatrix} -\dfrac{U_0\,\Gamma'}{\Gamma^2} & \dfrac{1}{\Gamma} \\ -\dfrac{{U_0}^2}{2}\left(\dfrac{\Gamma'}{\Gamma^2}\right)_\alpha & -\dfrac{U_0\Gamma'}{\Gamma^2} \end{bmatrix}, \tag{C2}$$

$$\boldsymbol{C} = \begin{bmatrix} 0 & 0 \\ \dfrac{\sigma D_{pipe}}{\rho_1} & 0 \end{bmatrix}, \tag{C3}$$

$$\boldsymbol{F}_\phi = \begin{bmatrix} 0 & 0 \\ F_{\alpha_2} & F_U \end{bmatrix}. \tag{C4}$$

REFERENCES

[1]W. D. Fullmer, G. Liu, X. Yin, and C. M. Hrenya, "Clustering instabilities in sedimenting fluid–solid systems: Critical," J. Fluid Mech. **823**, 433–469 (2017).
[2]S. Schneiderbauer and M. Saeedipour, "Approximate deconvolution model for the simulation of turbulent gas-solid flows: An *a priori* analysis," Phys. Fluids **30**(2), 023301 (2018).
[3]A. Vaidheeswaran and M. A. Lopez de Bertodano, "Stability and convergence of computational Eulerian two-fluid model for a bubble plume," Chem. Eng. Sci. **160**, 210 (2017).
[4]F. Chao, D. Liu, J. Shan, J. Gou, and P. Wu, "Development of temporal and spatial high-order schemes for two-fluid seven-equation two-pressure model and its applications in two-phase flow benchmark problems," Int. J. Numer. Methods Fluids **88**(4), 169–192 (2018).
[5]A. Clausse and M. Lopez de Bertodano, "Natural modes of the two-fluid model of two-phase flow," Phys. Fluids **33**, 033324 (2021).
[6]M. Ishii, *Thermo-Fluid Dynamic Theory of Two-Phase Flow* (Eyrolles, Paris, 1975).
[7]C. Pauchon and P. Smereka, "Momentum interactions in dispersed flow: An averaging and a variational approach," Int. J. Multiphase Flows **18**, 65–87 (1992).
[8]D. Gidaspow, "Round table discussion (RT-1-2): Modeling of two-phase flow," in Proceedings of 5th International Heat Transfer Conference, Tokyo, 1974.
[9]M. Lopez de Bertodano, W. Fullmer, A. Clausse, and V. Ransom, *Two-Fluid Model Stability, Simulation and Chaos* (Springer International Publishing, 2017).
[10]A. Vaidheeswaran, A. Clausse, W. D. Fullmer, R. Marino, and M. Lopez de Bertodano, "Chaos in stratified wavy fluid-fluid flow," Chaos **29**(033121), 033121–033127 (2019).
[11]T. Yatabe, T. Kanagawa, and T. Ayukai, "Theoretical elucidation of effect of drag force and translation of bubble on weakly nonlinear pressure waves in bubbly flows," Phys. Fluids **33**(3), 033315 (2021).
[12]J. Geurst, "Virtual mass in two-phase bubbly flow," Phys. A **129**(2), 233–261 (1985).
[13]G. B. Wallis, "On Geurst's equations for inertial coupling in two-phase flow," in *Two Phase Flows and Waves* (Springer-Verlag, 1989), pp. 150–164.
[14]G. B. Wallis, "Inertial coupling in two-phase flow: Macroscopic properties of suspensions in an inviscid fluid," Multiphase Sci. Technol. **5**(1), 239–361 (1990).
[15]J. D. Ramshaw and J. A. Trapp, "Characteristics, stability, and short-wavelength phenomena in two-phase flow equation systems," Nucl. Sci. Eng. **66**, 93–102 (1978).
[16]J. M. Saiz-Jabardo and J. A. Bouré, "Experiments on void fraction waves," Int. J. Multiphase Flow **15**(4), 483–493 (1989).
[17]J. W. Park, D. A. Drew, and R. T. Lahey, "The measurement of void waves in bubbly two-phase flows," Nucl. Eng. Des. **149**, 37–52 (1994).
[18]V. H. Ransom, "Summary of research on numerical methods for two-fluid modelling of two-phase flow," in Information Systems Laboratories (ISL) Report for USNRC Office of Regulatory Research, 2000.
[19]P. D. Lax and R. D. Richtmyer, "Survey of the stability of linear finite difference equations," Commun. Pure Appl. Math. **9**, 267–293 (1956).
[20]P. J. Roache, *Verification and Validation in Computational Science and Engineering* (Hermosa Publishers, Albuquerque, NM, 1998).
[21]G. B. Whitham, *Linear and Nonlinear Waves* (Wiley-Interscience, 1974).
[22]N. Zuber and J. A. Findlay, "Average volumetric concentration in two-phase flow systems," J. Heat Transfer **87**, 453–468 (1965).
[23]H. Cheng, J. H. Hills, and B. J. Azzopardi, "Effects of initial bubble size on flow pattern transition in a 28.9 mm diameter column," Int. J. Multiphase Flow **28**(6), 1047–1062 (2002).
[24]M. Ishii, "Thermally induced flow instabilities in two-phase thermal equilibrium," Ph.D. thesis (Georgia Institute of Technology, Atlanta, GA, 1971).
[25]M. Ishii and T. Chawla, *Local Drag Laws in Dispersed Two-Phase Flow* (Argonne National Lab Report, Lemont, 1979).
[26]G. B. Wallis, *One Dimensional Two-Phase Flow* (McGraw-Hill, New York, 1969).
[27]N. Waterson and H. Deconick, "Design principles for bounded higher-order convection schemes—A unified approach," J. Comput. Phys. **224**(1), 182–207 (2007).
[28]S. Gottileb and C. W. Shu, "Total variation diminishing Runge–Kutta schemes," Math. Comput. **67**(221), 73–85 (1998).